MALAYSIAN JOURNAL OF ANALYTICAL SCIENCES

Journal homepage: https://mjas.analis.com.my/

Research Article

Characterization and morphology of PdNiCo trimetallic MOF-derived porous carbon catalyst at different pyrolysis temperatures

Najihah Syahbudin[1], Muhammad Shafie Norhisham[1], Norliza Dzakaria[1,2*], Azizul Hakim Lahuri[3], Wan Nor Roslam Wan Isahak[4], Nurul Auni Zainal Abidin[1], Mohd Lokman Ibrahim[5], and Mohamad Azuwa Mohamed[6]

[1]School of Chemistry and Environment, Faculty of Applied Sciences, Universiti Teknologi MARA(UiTM), Cawangan Negeri Sembilan, Kampus Kuala Pilah, 72000 Kuala Pilah, Negeri Sembilan, Malaysia.
[2]Advanced Material for Environmental Remediation (AMER), Universiti Teknologi MARA(UiTM), Cawangan Negeri Sembilan, Kampus Kuala Pilah, 72000 Kuala Pilah, Negeri Sembilan, Malaysia.
[3]Department of Science and Technology, Universiti Putra Malaysia Sarawak, Nyabau Road, P.O Box 396, 97008 Bintulu, Sarawak, Malaysia.
[4]Department of Chemical and Process Engineering, Faculty of Engineering and Built Environment, Universiti Kebangsaan Malaysia, 43600 Bangi, Selangor, Malaysia.
[5]School of Chemistry and Environment, Faculty of Applied Sciences, Universiti Teknologi MARA (UiTM), 40450 Shah Alam, Selangor, Malaysia.
[6]Department of Chemical Sciences, Faculty of Science and Technology, Universiti Kebangsaan Malaysia, 43600 UKM Bangi, Selangor, Malaysia.

*Corresponding author: norliza864@uitm.edu.my

Received: 14 February 2026; Revised: 8 July 2026; Accepted: 27 July 2026; Published: 31 October 2026

Abstract

Efficient trimetallic catalysts require control of alloy formation, dispersion, and porous supports to maximize active-site accessibility for sustainable hydrogen generation. However, the influence of pyrolysis temperature on structural evolution of MOF-derived PdNiCo catalysts is not well understood. This study determines how pyrolysis temperature (500, 700, 900 °C) affects the structural, morphological, and textural properties of equimolar PdNiCo (1:1:1) supported on MOF-derived porous carbon and links these changes to catalytic performance for formic acid dehydrogenation. PdNiCo-MOF precursors were pyrolyzed at 500, 700, and 900 °C under 20% H_2/Ar. Materials were characterized by XRD, FESEM-EDX, CHNS, and N_2 adsorption-desorption analysis using the Brunauer-Emmett-Teller (BET) method. Catalytic activity and apparent activation energy were evaluated via batch formic acid dehydrogenation experiments. Properties were found to vary non-monotonically with temperature. XRD confirmed enhanced crystallinity and possible alloy formation at 900 °C. FESEM revealed particle coalescence at 700 °C and smaller primary particles (~146.6 nm) at 900 °C, while EDX confirmed Pd, Ni, and Co in all catalysts. CHNS analysis showed increased carbon content (12.20-14.53 wt%) and decreased nitrogen and hydrogen contents with increasing pyrolysis temperature, indicating progressive carbonization. PdNiCo/PC-900 showed the best combination of crystallinity and porosity with well-defined fcc metallic phases, highest BET surface area (40.92 $m^2\ g^{-1}$) and pore volume (0.117 $cm^3\ g^{-1}$), small primary particles (~146.6 nm), and lowest activation energy (≈19.3 kJ mol^{-1}) and TOF ≈ 104.48 h^{-1}, yielding the highest catalytic rates. PdNiCo/PC-700 represented a sintering window with severe particle coalescence, structural densification, and the lowest surface area (16.77 $m^2\ g^{-1}$). PdNiCo/PC-500 exhibited incomplete MOF decomposition and limited alloy crystallinity. Optimal performance requires balancing alloy crystallinity, controlled agglomeration, and hierarchical porosity. PdNiCo/PC-900 is hence identified as the preferred pyrolysis condition for producing high-performance PdNiCo trimetallic catalysts for sustainable hydrogen production.

Keywords: metal organic frameworks, trimetallic, pyrolysis temperature, porous carbon

Introduction

The growing demand for sustainable energy technologies has intensified interest in advanced catalytic materials capable of enhancing energy conversion and storage processes. Among various catalyst systems, multimetallic catalysts have attracted considerable attention due to their ability to exploit synergistic interactions between different metals, resulting in improved catalytic activity, selectivity, and stability. In particular, Pd-based trimetallic catalysts have emerged as promising candidates because the incorporation of Ni and Co can modify the electronic structure of Pd through alloying effects, thereby enhancing catalyst performance while reducing

reliance on expensive noble metals [1, 2].

Despite these advantages, trimetallic catalysts often suffer from particle agglomeration, phase separation, and poor metal dispersion, all of which limit active-site utilization and long-term stability. To overcome these challenges, the development of suitable support materials capable of stabilizing metallic nanoparticles while preserving synergistic metal-metal interactions is essential.

Metal-organic framework (MOF)-derived porous carbons have emerged as attractive catalyst supports owing to their high surface area, tunable porosity, and controllable structural properties. During pyrolysis, MOFs act as sacrificial templates that transform into porous carbon matrices while simultaneously facilitating the formation and confinement of metal nanoparticles within the carbon framework [3]. The resulting materials exhibit enhanced metal dispersion, improved metal-support interactions, and accessible pore networks that are advantageous for catalytic applications. Furthermore, heteroatoms inherited from MOF linkers can provide additional anchoring sites and contribute to structural stability [3].

Recent studies have demonstrated the effectiveness of MOF-derived carbon-supported metal catalysts, including Pd-, PdNi-, and PdCo-based systems, in improving alloy formation, electronic interactions, and resistance to nanoparticle agglomeration. However, most investigations have primarily focused on catalytic performance, while the temperature-dependent structural evolution of trimetallic MOF-derived catalysts remains insufficiently understood. In particular, systematic studies correlating pyrolysis temperature with alloy formation, crystallinity development, particle growth, pore evolution, and elemental redistribution in PdNiCo-containing MOF-derived carbon systems are still limited.

Pyrolysis temperature is a critical parameter governing the transformation of MOFs into porous carbon-supported catalysts. Variations in thermal treatment can significantly influence carbonization behavior, pore structure development, metal crystallization, alloy formation, and particle growth [4]. While lower temperatures generally preserve structural features of the parent MOF, higher temperatures promote metal crystallization and structural reorganization of the carbon matrix, which may either enhance or deteriorate the resulting physicochemical properties [5]. Consequently, identifying the optimum pyrolysis temperature is essential for tailoring the structure of MOF-derived trimetallic catalysts. Therefore, this study systematically investigates the structural and morphological evolution of equimolar PdNiCo (Pd:Ni:Co = 1:1:1) trimetallic catalysts supported on MOF-derived porous carbon and pyrolyzed at 500, 700, and 900 °C. Comprehensive characterization using X-ray diffraction (XRD), field-emission scanning electron microscopy (FESEM), energy-dispersive X-ray spectroscopy (EDX), and Brunauer-Emmett-Teller (BET) analysis was performed to elucidate the influence of pyrolysis temperature on crystallinity, morphology, elemental composition, and textural properties. The findings provide important insights into temperature-dependent structure-property relationships and establish a framework for the rational design of MOF-derived trimetallic catalysts for future energy-related applications.

Materials and Methods

Synthesis of PdNiCo-MOF using NH_2-BDC ligand

The trimetallic metal-organic framework (PdNiCo-MOF) was synthesized via a solvothermal method using an equimolar metal composition ratio (Pd:Ni:Co = 1:1:1). In a typical synthesis, 10 mg of 2-aminoterephthalic acid (NH_2-BDC) was mixed with palladium(II) nitrate hexahydrate ($Pd(NO_3)_2{\cdot}6H_2O$), nickel(II) nitrate hexahydrate ($Ni(NO_3)_2{\cdot}6H_2O$), and cobalt(II) nitrate hexahydrate ($Co(NO_3)_2{\cdot}6H_2O$) in equal proportions to ensure uniform incorporation of the three metallic species within the MOF framework. Specifically, 8 mg of each metal precursor was added into a 20 mL glass vial containing a solvent mixture of 3.0 mL dimethyl sulfoxide (DMSO), 0.2 mL methanol (MeOH), and 0.04 mL of 1.4 M HNO_3 in dimethylformamide (DMF). DMSO was used as the primary high-boiling polar aprotic solvent to dissolve reactants and facilitate coordination, MeOH (small co-solvent) improved precursor solubility and moderated nucleation, and the small volume of 1.4 M HNO_3 in DMF served as an acid modulator to control proton activity and direct crystallization. The resulting mixture was ultrasonically dispersed until a homogeneous solution was obtained, sealed, and transferred into a preheated oven at 110 °C for 48 hours under static conditions. These temperature and time conditions were chosen based on preliminary optimization and literature precedent as 110 °C provides sufficient thermal energy for ligand exchange and framework crystallization without decomposition, and 48 hours was found to consistently produce phase-pure crystalline material while shorter times gave incomplete crystallization [6].

After naturally cooling to room temperature, the solid product was recovered by filtration and repeatedly washed with DMF and dichloromethane (CH_2Cl_2) to remove residual reactants and solvent molecules. The purified product was subsequently dried at 60 °C for 2 hours, yielding a yellow-brown crystalline PdNiCo-MOF. The typical product yield was approximately 80-90% based on the initial ligand amount.

Preparation of porous carbon materials of PdNiCo at different temperatures

The derived porous carbon materials were prepared

through controlled thermal treatment of the corresponding MOF precursors. The as-synthesized PdNiCo-MOF was separately placed in a quartz boat and transferred into a tube furnace under a continuous flow of 20% H_2/Ar gas mixture. The samples were heated directly to the desired temperature (500, 700, and 900 °C) at a ramping rate of 5 °C min^{-1}, followed by a holding period of 2 hours at the target temperature.

Upon completion of the calcination, the products were allowed to cool naturally to room temperature under the protective gas flow. The resulting carbonaceous materials were denoted as PdNiCo/PC-500, PdNiCo/PC-700, and PdNiCo/PC-900 (from PdNiCo-MOF).

Characterization catalysts PdNiCo-NH_2BDC and PdNiCo-UiO-66-NH_2

X-ray diffraction

The physicochemical properties of the prepared catalyst were characterized by X-ray diffraction (XRD), using the Cu Kα X-ray radiation source (40 kV, 40 mA) in the XRD Bruker AXS D8 (Advance type) to record the 2θ diffraction angle from 5° to 80° at a wavelength of (λ = 0.154 nm). The diffractogram was matched with the JCPDS file to identify the crystalline phase composition.

Field emission scanning electron microscope (FESEM-EDX)

To identify the surface micrograph of the prepared catalyst, the ZEISS Supra VP55 type field emission scanning electron microscope (FESEM) was used. This instrument uses a tungsten-type electron gun with a voltage range of 0.1 to 3.0 kV. The microscope has a radiation detector for mapping elements. The sample also underwent EDX analysis to assess the position and distribution of the components within the sample.

Nitrogen adsorption-desorption isotherm (BET)

Nitrogen gas isothermal adsorption testing was conducted using the BET method to analyze the physical surface attributes of the prepared catalyst, specifically its nitrogen gas adsorption capacity. Surface area measurements were determined by the Brunauer, Emmett, and Teller (BET) model using a Micromeritics ASAP 2020 analyzer. For the analysis, 0.3-1.0 g of catalyst was degassed in a glass tube under vacuum (20 torr) at 300 °C for 4 hours. Nitrogen gas (N_2) was then adsorbed onto the catalyst surface at -196 °C (77K), forming monolayers, multilayers, and eventually condensation. The BET model provided the sample surface area (SBET), using the linear portion of the BET plot within the P/Po range of 0.05 to 0.30. Additionally, the Barrett-Joyner-Halenda (BJH) method was applied to automatically calculate the pore volume (V_{pore}) and average pore diameter (D_{pore}) using the Micromeritics ASAP 2020 software.

Catalytic reaction towards formic acid decomposition

The catalytic performance of the synthesized PdNiCo catalysts toward formic acid (FA) decomposition was evaluated using a batch reaction system coupled with a gas collection apparatus based on the water displacement method. The experimental setup consisted of a 25 mL two-neck round-bottom flask connected via a rubber tube to an inverted water-filled graduated cylinder for measuring the cumulative volume of evolved gas. A magnetic stirrer operating at 600 rpm was used throughout the reaction to ensure homogeneous catalyst dispersion and minimize external mass transfer limitations. All experiments were conducted under ambient atmospheric conditions without inert gas purging.

For each experiment, 0.03 g of the catalyst (PdNiCo/PC-500, PdNiCo/PC-700, or PdNiCo/PC-900) was placed in the reaction flask. The catalyst loading was maintained constant throughout the study to enable a direct comparison of the catalytic performance of the three catalysts prepared at different calcination temperatures. Formic acid solutions with concentrations of 1.0, 3.0, and 5.0 M were prepared by diluting concentrated formic acid (98 wt%) with deionized water. A fixed volume of 1 mL of the prepared FA solution was introduced into the reaction flask to initiate the catalytic reaction. The selected FA concentrations were chosen to investigate the influence of reactant concentration on the catalytic decomposition behavior.

The catalytic reactions were carried out at 30, 50, and 70 °C using a thermostatically controlled oil bath to maintain a constant reaction temperature throughout the experiment. These temperatures were selected to evaluate the influence of thermal energy on the catalytic performance under mild reaction conditions.

The volume of evolved gas was monitored using the water displacement method and recorded at 5 minutes intervals over a total reaction time of 30 minutes (0, 5, 10, 15, 20, 25, and 30 minutes). The cumulative gas volume was used as an indicator of catalytic activity toward FA decomposition. Blank experiments conducted under identical conditions in the absence of catalyst showed negligible gas evolution, confirming that the measured gas originated predominantly from the catalytic reaction. Each experiment was performed in duplicates to ensure reproducibility, and the average values were reported.

Results and Discussion

XRD analysis

The X-ray diffraction (XRD) patterns of the PdNiCo-MOF precursor and its pyrolyzed derivatives (PdNiCo/PC-500, PdNiCo/PC-700, and PdNiCo/PC-900) are presented in **Figure 1**. The pristine PdNiCo-MOF exhibited a broad diffraction profile with no

distinct sharp reflections, indicating the predominantly amorphous nature of the framework and the homogeneous dispersion of Pd, Ni, and Co species within the MOF structure. Furthermore, no characteristic diffraction peaks associated with graphitic carbon were observed in the pyrolyzed samples, suggesting that the carbon generated during pyrolysis remained largely amorphous under the applied carbonization temperatures (<1000 °C).

Following pyrolysis at 500 °C, weak diffraction peaks emerged at approximately 2θ = 40.2°, 44.3°, and 46.6°. The reflection at 40.2° corresponds closely to the characteristic Pd(111) plane, while the peak at 46.6° is consistent with the Pd(200) reflection (JCPDS No. 65-2867). A reflection centred around 44.3° is located near the standard position of Ni(111) (JCPDS No. 04-0850). However, due to the overlap of Pd, Ni, and Co reflections in this region, definitive phase assignment remains difficult. The broad and low-intensity nature of these peaks indicates incomplete crystallization, small crystallite size, and limited alloy development at this temperature. The absence of distinct Ni- and Co-related reflections further suggests that these species remain highly dispersed within the carbon matrix.

Upon increasing the pyrolysis temperature to 700 °C, the diffraction peaks became sharper and more intense, indicating enhanced crystallization and particle growth. The diffraction feature within the 2θ range of 40-45° shifted slightly towards higher diffraction angles relative to monometallic Pd (2θ ≈ 40.1°). Such peak displacement is commonly associated with lattice contraction resulting from the incorporation of smaller Ni and Co atoms into the Pd lattice, suggesting the formation of a Pd-based alloy phase. Similar peak shifts have been reported for Pd-Ni and Pd-Co alloy systems, where alloying induces changes in lattice parameters and electronic structure. The PdNiCo/PC-900 sample exhibited the highest crystallinity among all the investigated catalysts, as evidenced by the significantly increased peak intensity and reduced peak broadening. Strong reflections were observed within the 2θ range of approximately 40-45°, indicating the development of well-defined metallic phases. The pronounced peak broadening observed at lower temperatures was substantially reduced after pyrolysis at 900 °C, reflecting improved long-range atomic ordering and crystal growth. Additional reflections were detected at approximately 49.7° and 77.6°, which indicate further crystallization of metallic species. However, precise assignment of these reflections is challenging due to the overlap of Pd-, Ni-, and Co-related phases and the possible presence of alloy-induced peak shifts. The appearance of a shoulder peak near 42.1° may be associated with lattice distortion arising from alloy formation and the interaction between the Pd, Ni, and Co species. Collectively, these observations suggest that higher pyrolysis temperatures promote metal reduction, crystallization, and alloy development within the MOF-derived carbon framework.

The progressive sharpening of diffraction peaks and their slight displacement towards higher diffraction angles with increasing pyrolysis temperature indicate enhanced crystallization and stronger interaction among Pd, Ni, and Co species. The XRD results therefore provide evidence for the evolution of Pd-based alloy structures during pyrolysis, with PdNiCo/PC-900 exhibiting the highest degree of crystallinity and the most pronounced alloy characteristics among the investigated samples.

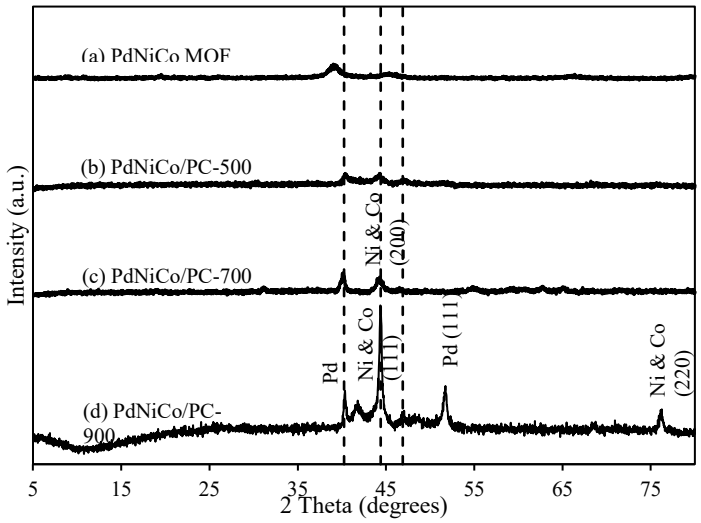


Figure 1. XRD patterns of PdNiCo MOF-derived catalysts for (a) PdNiCo MOF, (b) PdNiCo/PC-500, (c) PdNiCo/PC-700, and (d) PdNiCo/PC-900

Nitrogen adsorption-desorption isotherm (BET)

The textural properties of the PdNiCo MOF-derived porous carbon catalysts were investigated using N_2 adsorption-desorption measurements, as presented in **Figure 2**, while the corresponding BET surface area, pore volume, and average pore diameter are summarized in **Table 1**. All samples exhibited Type IV adsorption-desorption isotherms according to the IUPAC classification, confirming the predominance of mesoporous structures. A distinct hysteresis loop was observed at relative pressures (P/P_0) above approximately 0.8, indicating capillary condensation within mesopores. The hysteresis profile resembles an H3/H4-type loop, which is commonly associated with slit-shaped pores generated from the aggregation of carbonaceous frameworks and metallic nanoparticles.

Among the investigated samples, PdNiCo/PC-900 exhibited the highest N_2 uptake at elevated relative pressures, indicating the largest accessible pore volume and the most developed porous architecture. In contrast, PdNiCo/PC-700 displayed the lowest adsorption capacity throughout the measured pressure range, suggesting partial pore collapse and structural densification during pyrolysis. PdNiCo/PC-500 exhibited intermediate adsorption behavior, indicating incomplete pore development due to insufficient decomposition and restructuring of the MOF framework.

The BET surface area followed the order of PdNiCo/PC-900 (40.92 $m^2\ g^{-1}$), PdNiCo/PC-500 (32.48 $m^2\ g^{-1}$), and PdNiCo/PC-700 (16.77 $m^2\ g^{-1}$). A similar trend was observed for the cumulative pore volume, where PdNiCo/PC-900 possessed the highest pore volume (0.117 $cm^3\ g^{-1}$), followed by PdNiCo/PC-500 (0.086 $cm^3\ g^{-1}$) and PdNiCo/PC-700 (0.059 $cm^3\ g^{-1}$). The reduced surface area and pore volume observed for PdNiCo/PC-700 can be attributed to framework shrinkage, particle coalescence, and partial blockage of pore channels during intermediate-temperature pyrolysis. Upon increasing the pyrolysis temperature to 900 °C, further decomposition and reorganization of the MOF-derived carbon framework promoted pore reopening and the generation of additional accessible porosity, resulting in a more developed mesoporous network. These observations are consistent with the pore size distribution results, which showed that PdNiCo/PC-900 possessed the highest differential pore volume and the most pronounced mesoporous characteristics.

Overall, the nitrogen adsorption-desorption isotherm analysis demonstrates that pyrolysis temperature significantly influences the evolution of the porous structure. The textural properties of PdNiCo/PC-900 arise from enhanced pore development and increased pore accessibility rather than the formation of highly graphitized carbon, which is consistent with the XRD results indicating a predominantly amorphous carbon matrix.

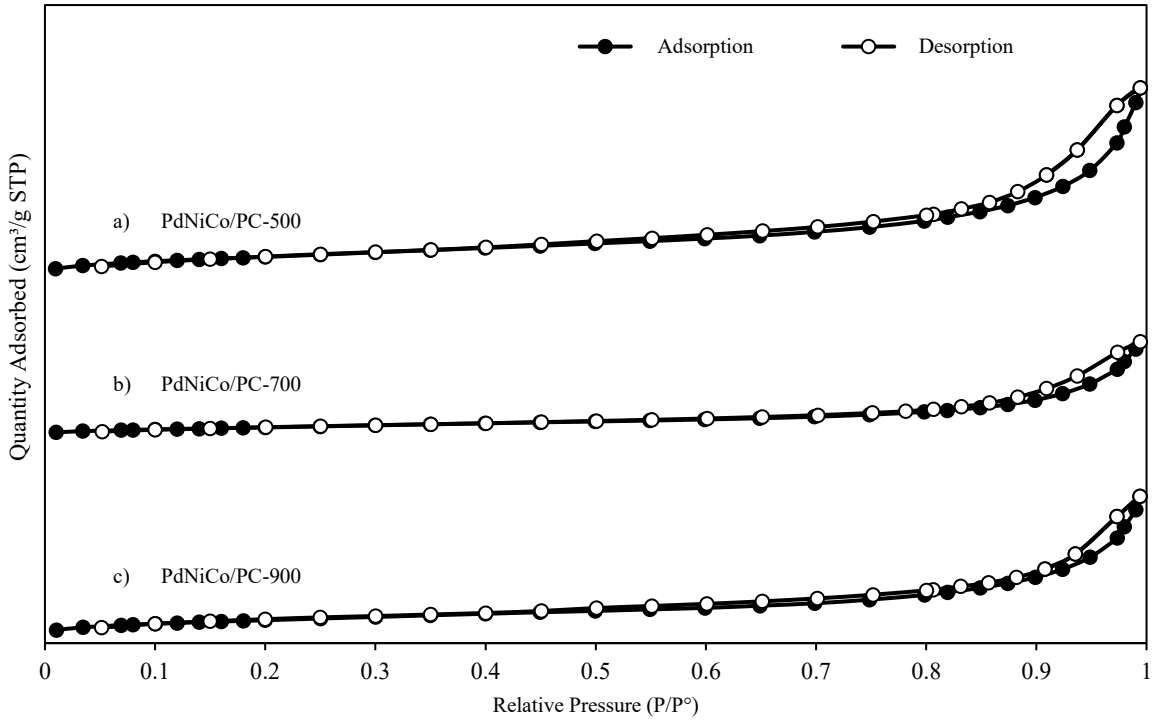


Figure 2. N_2 adsorption-desorption isotherms of PdNiCo catalysts for (a) PdNiCo/PC-500, (b) PdNiCo/PC-700,

and (c) PdNiCo/PC-900

Table 1. Textural properties of PdNiCo catalysts prepared at different pyrolysis temperatures

Catalyst	BET Surface Area (m^2/g)	Total Pore Volume (cm^3/g)	Langmuir Surface Area (m^2/g)	BJH Cumulative Pore Volume (cm^3/g)	Average Pore Diameter (nm)	Particle Size Range
PdNiCo/PC-500	32.48	0.052	70.74	0.086	6.46	0.5-5 µm (aggregate)
PdNiCo/PC-700	16.77	0.034	38.20	0.059	8.04	100-500 nm
PdNiCo/PC-900	40.92	0.071	96.00	0.117	6.89	50-200 nm

The pore size distribution for PdNiCo/PC-500, PdNiCo/PC-700, and PdNiCo/PC-900 was computed using the BJH method, as shown in **Figure 3**. Meanwhile, **Table 2** shows the comparative analyses of the catalyst properties. All samples demonstrate a broad pore size distribution ranging from approximately 3 to 70 nm, confirming the hierarchical porous nature of the MOF-derived carbon materials. According to the IUPAC classification, pores with diameters in the range of 2-50 nm are categorized as mesopores, while pores larger than 50 nm are classified as macropores.

For PdNiCo/PC-500, the pore size distribution is mainly concentrated in the small mesopore region (≈5-15 nm), originating from partial decomposition of organic linkers and limited metal-induced pore expansion. The relatively low intensity of the pore distribution curve at larger pore widths suggests restricted macropore formation at this temperature. In contrast, PdNiCo/PC-700 exhibits the lowest intensity across both mesopore and macropore regions, which correlates well with its reduced BET surface area and pore volume. This phenomenon can be attributed to pore wall collapse and densification of the carbon matrix, where thermal energy is sufficient to destroy microporous structures but insufficient to generate new macropores [7].

PdNiCo/PC-900 shows significantly enhanced pore volume with pronounced peaks in both the mesopore (10-30 nm) and macropore (30-60 nm) regions. The higher intensity of the pore size distribution curve indicates the formation of interconnected hierarchical pores, likely caused by rapid gas release, metal nanoparticle migration, and carbon framework reconstruction at high temperature. This porous evolution facilitates improved mass transport and accessibility of active Pd-Ni-Co sites, which is beneficial for catalytic applications such as formic acid dehydrogenation [8]. The presence of broad macropores alongside mesopores suggests that PdNiCo nanoparticles are well dispersed on the carbon surface rather than embedded within the pore walls, preserving pore accessibility even at high metal loading. This observation is consistent with MOF-derived systems, where metal nodes act as in-situ pore formers during high-temperature carbonization.

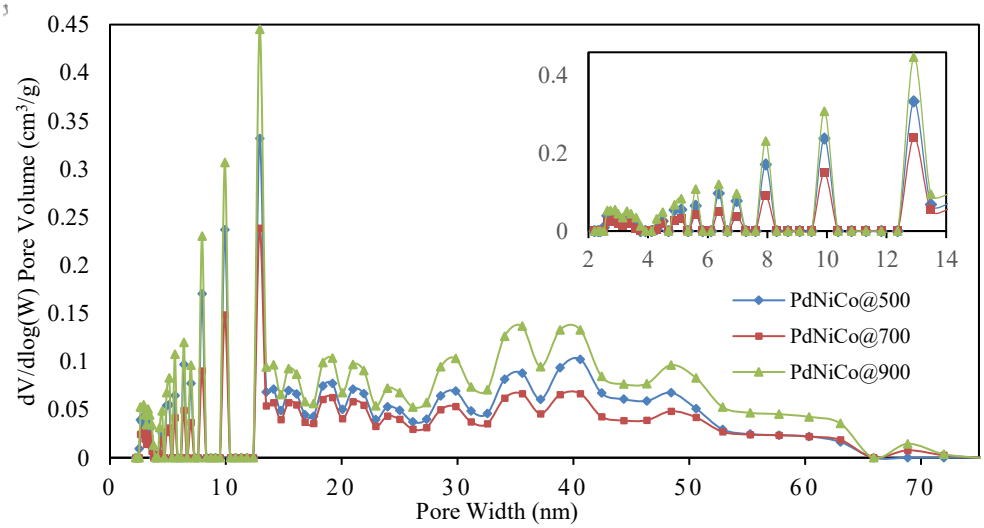


Figure 3. Pore size distribution of PdNiCo catalysts for (a) PdNiCo/PC-500, (b) PdNiCo/PC-700, and (c) PdNiCo/PC-900

Table 2. Dominant pore size distribution peaks of PdNiCo catalysts derived from UiO-66 at different pyrolysis temperatures

Sample	Dominant Pore Width (nm)	Maximum dV/dlog(W) ($cm^3\ g^{-1}$)	Secondary Mesopore Region (nm)
PdNiCo/PC-500	12.91	0.332	34-41
PdNiCo/PC-700	12.91	0.239	34-41
PdNiCo/PC-900	12.91	0.445	34-41

FESEM-EDX morphology analysis

The morphological characteristics for PdNiCo/PC-500, PdNiCo/PC-700, and PdNiCo/PC-900 were examined by field-emission scanning electron microscopy (FESEM), and the corresponding images are presented in **Figure 4.** The FESEM results reveal pronounced morphology evolution as a function of pyrolysis temperature, which correlates well with the trends observed in the BET surface area and XRD crystallinity analyses.

The PdNiCo/PC-500 (**Figure 4a**) exhibits irregularly shaped particles with an average particle size of 184.73 nm. The particles show a broad size distribution with moderate agglomeration and discernible inter-particle voids. The surface texture is rough and heterogeneous, indicating partial decomposition of the MOF precursor at this temperature. Remnant MOF-derived structural features can still be inferred, suggesting that carbonization and metal reduction are incomplete at 500 °C. The presence of inter-particle voids contributes to moderate porosity, which is consistent with the measured BET surface area of 32.48 $m^2\ g^{-1}$. However, the non-uniform morphology and irregular particle shapes imply limited structural optimization at this temperature.

Upon increasing the pyrolysis temperature to 700 °C (**Figure 4b**), significant morphological changes are observed. The PdNiCo/PC-700 displays the largest average particle size of 357.78 nm, corresponding to an increase of approximately 93% relative to PdNiCo/PC-500. The particles are densely agglomerated with minimal inter-particle spacing, forming compact aggregates with smoother surfaces. This morphological densification is indicative of pronounced particle coalescence and sintering driven by enhanced atomic diffusion at intermediate temperatures. The dense packing and reduced pore accessibility are in excellent agreement with the lowest BET surface area (16.77 $m^2\ g^{-1}$) among all samples. These results suggest that 700 °C represents a critical temperature regime where particle growth and sintering dominate over pore development, leading to unfavorable structural characteristics for catalytic applications [9].

In contrast, the PdNiCo/PC-900 sample (**Figure 4c**) exhibits the most favorable morphology. The average particle size decreases markedly to 146.64 nm, representing a 59% reduction compared to the PdNiCo/PC-700 sample. Although particle agglomeration remains evident, the nature of the agglomeration differs substantially from that observed at PdNiCo/PC-700. Rather than forming dense, compact clusters, the particles assemble into open, more loosely packed particle assemblies composed of uniformly distributed small primary particles. The resulting structure displays a sponge-like, morphological feature consistent with improved pore development with extensive inter-particle connectivity [10]. This morphology provides highly accessible porosity and efficient mass transport pathways, consistent with the highest BET surface area of 40.92 $m^2\ g^{-1}$ measured for this sample. The improved porosity can be attributed to enhanced carbon framework stabilization and stronger metal-support interactions at high pyrolysis temperatures which suppress excessive particle growth despite increased thermal energy.

The observed morphological evolution can be rationalized by temperature-dependent structural processes. At 500 °C, incomplete MOF decomposition leads to irregular particles with moderate porosity. At 700 °C, enhanced atomic mobility promotes particle coalescence and sintering, causing pore collapse and structural densification. At 900 °C, further carbonization and structural reorganization of the carbon framework promote pore development and suppress excessive particle coalescence, while strong metal-carbon interactions limit excessive sintering and promote the formation of interconnected porous networks. Similar non-monotonic morphology evolution has been reported for MOF-derived multimetallic catalysts subjected to high-temperature pyrolysis, where optimized thermal treatment balances metal dispersion, particle growth, and pore preservation [11].

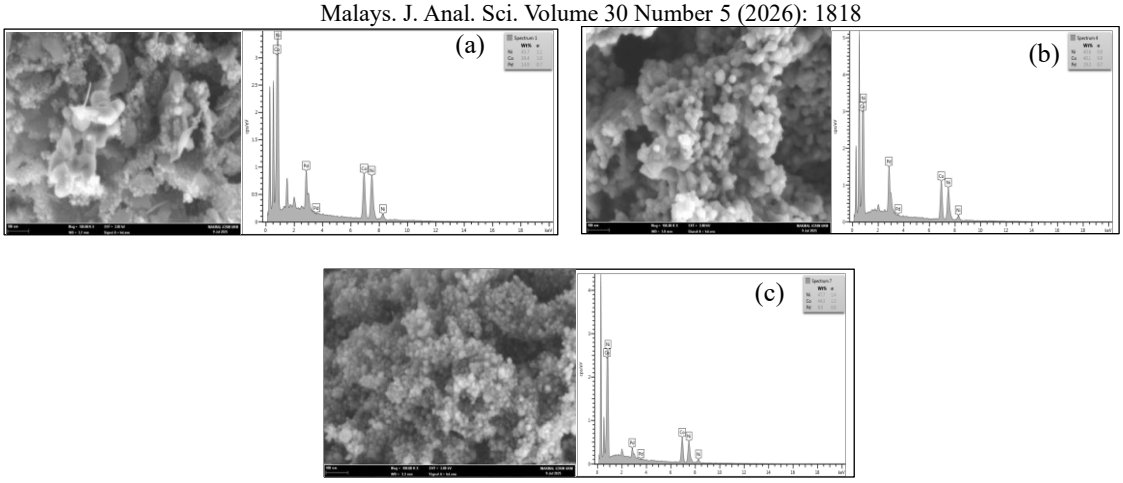


Figure 4. FESEM images of PdNiCo catalysts for (a) PdNiCo/PC-500 (b) PdNiCo/PC-700, and (c) PdNiCo/PC-900

Table 3. EDX elemental composition of PdNiCo catalysts at different calcination temperatures

Sample	C (wt%)	Ni (wt%)	Co (wt%)	Pd (wt%)
PdNiCo/PC-500	69.4	14.1	1.6	14.9
PdNiCo/PC-700	40.1	6.9	11.9	23.7
PdNiCo/PC-900	44.3	1.3	0.8	53.6

The elemental composition of PdNiCo catalysts was further investigated using EDX analysis, as summarized in **Table 3**. The spectra confirm the presence of Pd, Ni, and Co in all calcined samples, demonstrating successful incorporation of the three metallic species within the carbon matrix. PdNiCo/PC-500 exhibits comparable Pd and Ni contents (14.9 and 14.1 wt%, respectively), whereas PdNiCo/PC-700 shows a relatively higher Pd content (23.7 wt%) accompanied by increased Co concentration (11.9 wt%). Upon increasing the calcination temperature to 900 °C, the Pd content increased significantly to 53.6 wt%, while the Ni and Co contents decreased to 1.3 and 0.8 wt%, respectively. This trend suggests possible metal migration, particle growth, and partial loss or encapsulation of Ni and Co species during high-temperature treatment. Nevertheless, the simultaneous detection of Pd, Ni, and Co in all samples confirms successful trimetallic catalyst formation.

Elemental analysis

The elemental composition of PdNiCo/PC-500, PdNiCo/PC-700, and PdNiCo/PC-900 was determined by CHNS elemental analysis, and the results are summarized in **Table 4**. CHNS analysis quantifies only carbon (C), hydrogen (H), and nitrogen (N). Therefore, the reported weight percentages exclude the metallic components (Pd, Ni, and Co). Consequently, the CHNS values represent only the non-metallic elements within the catalyst and should not be interpreted as the total elemental composition.

PdNiCo/PC-500 exhibits carbon, nitrogen, and hydrogen contents of 12.20, 1.42, and 1.46 wt%, respectively, indicating the retention of carbonaceous species originating from the organic linker after pyrolysis at 500 °C. Upon increasing the calcination temperature to 900 °C, the carbon content increased to 14.53 wt%, whereas the nitrogen and hydrogen contents decreased to 0.96 wt% and 0.366 wt%, respectively. The decrease in nitrogen and hydrogen is consistent with the progressive elimination of volatile nitrogen- and hydrogen-containing functional groups during thermal decomposition, while the relatively higher carbon content suggests the formation of a more carbonized framework at elevated temperature.

In contrast, PdNiCo/PC-700 exhibits significantly lower carbon, nitrogen, and hydrogen contents of 0.97, 0.558, and 0.147 wt%, respectively. Such a substantial reduction in carbon content is inconsistent with the complementary characterization results. The FESEM images reveal that the catalyst morphology remains intact after calcination, while XRD and EDX analyses confirm the presence of the MOF-derived catalyst containing Pd, Ni, Co, and a carbonaceous matrix. Therefore, the unusually low CHNS values obtained for PdNiCo/PC-700 are more likely attributable to sample heterogeneity, incomplete sample homogenization, or analytical uncertainty rather than representing the actual bulk composition of the catalyst. As this observation is not supported by the other characterization techniques, no mechanistic interpretation is drawn based solely on the CHNS results. Repeated CHNS measurements or

complementary quantitative elemental analyses are recommended to verify the composition of this sample.

The calculated C/N ratio increased from 8.59 for PdNiCo/PC-500 to 15.13 for PdNiCo/PC-900, indicating progressive carbon enrichment relative to nitrogen with increasing calcination temperature. This trend suggests a higher degree of carbonization accompanied by the removal of nitrogen-containing functionalities, which is commonly associated with improved thermal stability and a more condensed carbon framework in MOF-derived porous carbon materials. In contrast, the low C/N ratio of 1.73 for PdNiCo/PC-700 reflects the anomalously low carbon content measured by CHNS and should therefore be interpreted with caution.

Catalytic dehydrogenation of FA

The catalytic activity of the MOF-derived PdNiCo/PC catalysts towards formic acid (FA) dehydrogenation is strongly governed by pyrolysis temperature, giving a consistent performance order of PdNiCo/PC-900, PdNiCo/PC-700 and PdNiCo/PC-500 across all reaction temperatures (30-70 °C), displayed in **Figures 5-7**. The higher gas-evolution rates of PdNiCo/PC-900 and its activation energy value (19.29 kJ mol^{-1}) indicate that this catalyst provides both faster intrinsic kinetics and more effectively accessible active sites. This superior behavior aligns with its optimized structure as PdNiCo/PC-900 exhibits the highest BET surface area (40.92 m^2 g^{-1}) and pore volume (0.117 cm^3 g^{-1}) with enhanced hierarchical meso and macroporosity, which improves FA diffusion to active sites and facilitates rapid removal of gaseous products, minimizing transport limitations. In parallel, XRD peak sharpening and shifts at higher temperatures suggest improved reduction and alloy development within a Pd-based fcc phase, which can electronically modify Pd through Ni/Co incorporation and generate more active ensembles for selective dehydrogenation. FESEM further supports this structure-activity relationship, showing that PdNiCo/PC-900 forms smaller primary particles (357.8 nm) and the lowest BET area (16.77 m^2 g^{-1}), consistent with pore collapse/blocked accessibility and therefore reduced activity despite improved crystallinity relative to PdNiCo/PC-500. PdNiCo/PC-500 retains moderate surface area (32.48 m^2 g^{-1}) but shows weaker crystallinity and incomplete MOF decomposition, limiting alloy formation and active-site quality, resulting in the lowest reaction rates. Overall, the synchronized kinetic and characterization results demonstrate that catalytic activity is maximized when alloy crystallinity is developed without sacrificing dispersion and hierarchical porosity, conditions best achieved at PdNiCo/PC-900.

Increasing of the pyrolysis temperature from 500 to 700 °C markedly enhances the catalytic activity, as evidenced by an increase in the initial rate from 0.40 to 0.60 mL min^{-1} and a proportional rise in TOF from 69.65 to 104.48 h^{-1}. This indicates that the performance improvement is not only due to a larger number of accessible sites, but also to higher intrinsic activity per active site, consistent with the more developed metallic phase/alloy features observed at higher pyrolysis temperature (sharper XRD reflections) and improved catalyst microstructure. In contrast, PdNiCo/PC-900 shows the same initial rate and TOF as PdNiCo/PC-700 in this dataset, implying that under the specific conditions, the intrinsic site activity (TOF) has reached a plateau between PdNiCo/PC-700 and PdNiCo/PC-900. Therefore, any additional structural advantages of the PdNiCo/PC-900 material, such as the higher BET surface area, larger pore volume, and smaller primary particles in a more open porous network may contribute more strongly under other operating conditions. Although these results suggest that PdNiCo/PC-700 is sufficient to achieve the maximum intrinsic activity captured, PdNiCo/PC-900 may still offer benefits in sustained performance and robustness by providing higher porosity and improved transport, which can help maintain high rates at higher conversions and during reuse.

Table 4. Elemental composition for PdNiCo/PC-500, PdNiCo/PC-700, and PdNiCo/PC-900

Sample	Elemental Composition (wt%)			
	C	N	H	C/N ratio
PdNiCo/PC-500	12.20	1.42	1.46	8.59
PdNiCo/PC-700	0.97	0.558	0.147	1.73
PdNiCo/PC-900	14.53	0.96	0.366	15.13

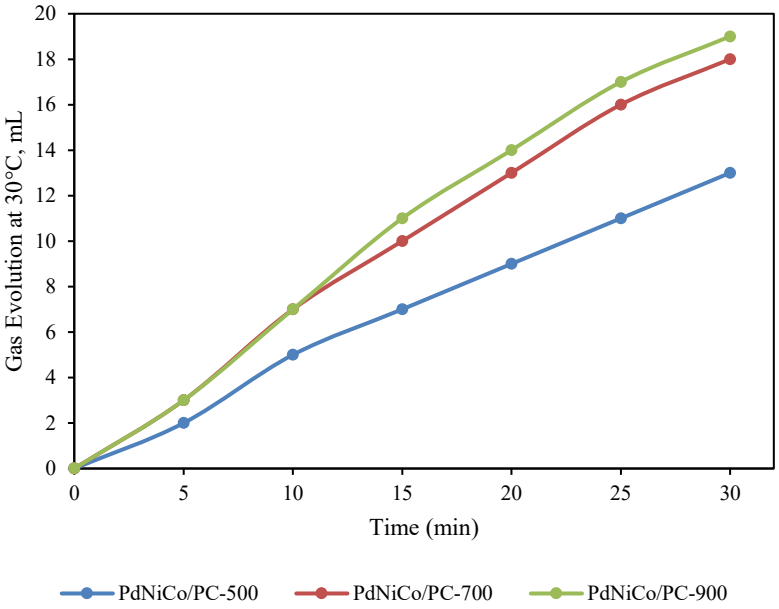


Figure 5. Volume of the generated gas vs. time for the dehydrogenation of FA over the PdNiCo/PC-500, PdNiCo/PC-700 and PdNiCo/PC-900

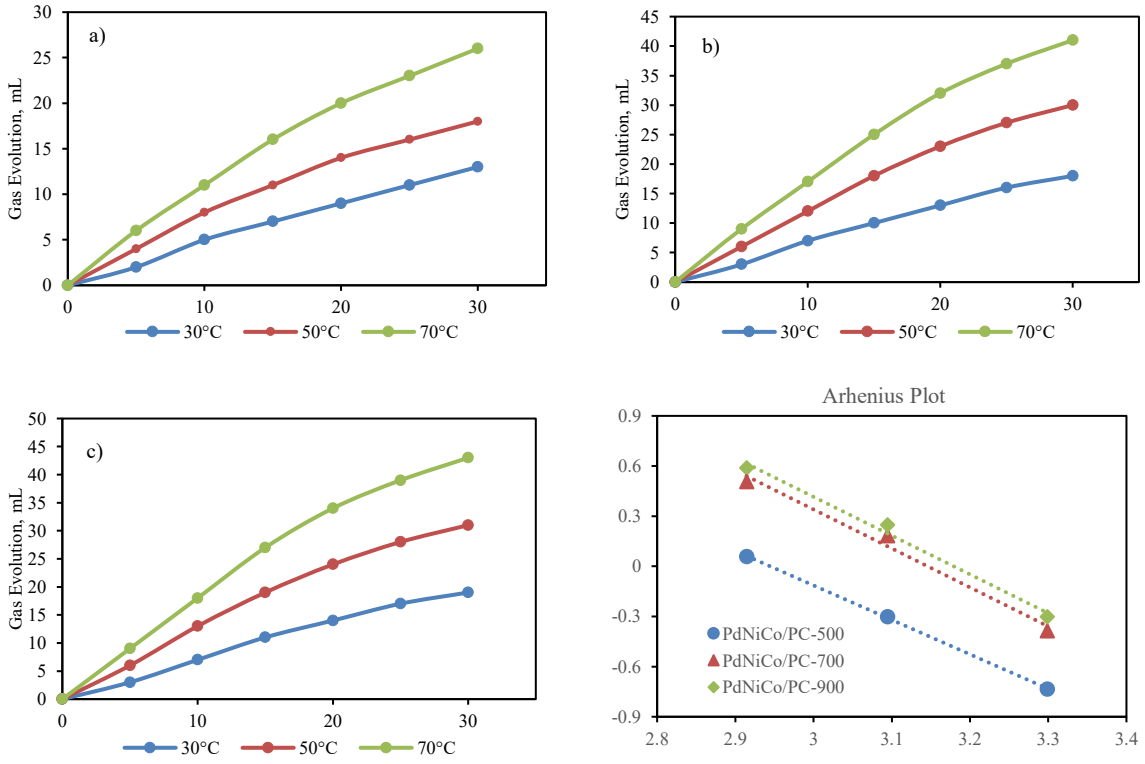


Figure 6. Volume of the generated gas vs. time for the dehydrogenation of FA over the (a) PdNiCo/PC-500, (b) PdNiCo/PC-700 and (c) PdNiCo/PC-900 with different reaction temperatures, and (d) Arrhenius plots of PdNiCo/PC-500, PdNiCo/PC-700 and PdNiCo/PC-900

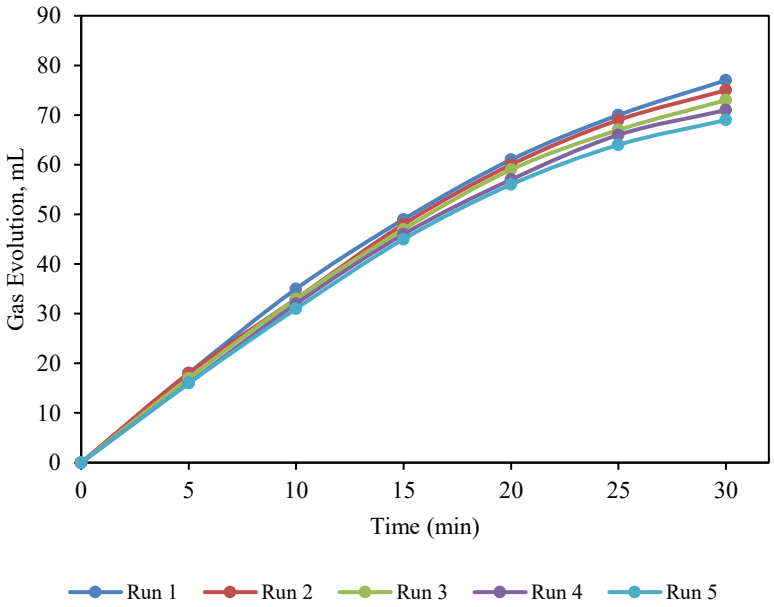


Figure 7. Volume of the generated gas versus time for the dehydrogenation of FA in stability test over PdNiCo/PC-900

Conclusion

This study reveals the non-monotonic dependence of MOF-derived PdNiCo catalyst properties on pyrolysis temperature and identifies 900 °C as the optimal condition. PdNiCo/PC-900 combines high crystallinity with well-defined fcc metallic phases, a pronounced hierarchical porous architecture (interconnected meso- and macropores), the largest BET surface area (40.92 m^2 g^{-1}) and pore volume (0.117 cm^3 g^{-1}), and small primary particles (104.48 h^{-1} observed at 700 °C). PdNiCo/PC-900 also shows low activation energy (Ea ≈ 19.29 kJ mol^{-1}), consistent with faster intrinsic kinetics. In contrast, PdNiCo/PC-700 is a detrimental sintering window (BET, 16.77 m^2 g^{-1}, particle size ~357.8 nm, pore collapse), while PdNiCo/PC-500 yields incomplete MOF decomposition and limited alloy/crystallinity. These results demonstrate that combining controlled alloy formation with preserved hierarchical porosity and limited agglomeration is critical to maximize accessible active sites and catalytic efficiency. Future work should probe long-term stability, detailed alloy-phase mapping, and performance under application-relevant conditions to further correlate hierarchical structure with durability and activity.

Acknowledgement

The authors would like to thank Universiti Teknologi MARA (UiTM) and the Ministry of Higher Education Malaysia for funding this project under research grant code FRGS/1/2023/STG05/UiTM/02/4 and the Centre of Research and Innovation Management of UKM (i-CRIM) for providing access to the instrument facilities.

References

1. Al-Aqtash, O., Sápi, A., Farkas, F., Basheer, H. S., Kukovecz, Á., & Kónya, Z. (2025). Enhanced performance and cost-effectiveness of Pd-based catalysts with Cu, Ni, and Co promoters for CO and NOx conversion in flue gas emission. *Atmospheric Pollution Research,* 16, 102579.
2. Bumagin, N. A. (2022). Reusable proline-containing bimetallic Pd–Ni(Co, Cu, Fe)–Pro/Al_2O_3 catalysts for Suzuki reaction in water. *Russian Journal of General Chemistry,* 92, 832–840.
3. Ding, J., Wang, H. F., Yang, X., Ju, W., Shen, K., Chen, L., & Li, Y. (2023). A Janus heteroatom-doped carbon electrocatalyst for hydrazine oxidation. *National Science Review,* 10, 231.
4. Castillo-Blas, C., Chester, A. M., Keen, D. A., & Bennett, T. D. (2024). Thermally activated structural phase transitions and processes in metal-organic frameworks. *Chemical Society Reviews*, 53(7), 3606-3629.
5. Hernández-Ferrer, J., Gracia-Martín, M., Benito, A. M., Maser, W. K., & García-Bordejé, E. (2023). Effect of temperature and presence of minor amount of metal on porous carbon materials derived from ZIF8 pyrolysis for electrocatalysis. *Catalysis Today,* 423, 024.
6. Hintz, H., & Wuttke, S. (2014). Supporting information: Postsynthetic modification of an amino-tagged MOF using peptide coupling reagents: A comparative study. *Chemical communications*, 50(78), 11472-11475.
7. Wang, Y., & Zhang, Q. (2023). Temperature-dependent tailoring of the pore structure based on MOF-derived carbon electrodes for electrochemical capacitors. *RSC Advances,* 13,

18145–18155.

8. Landström, K. N., Nambi, A., Kaiser, A., & Akhtar, F. (2023). Inducing hierarchical pores in nano-MOFs for efficient gas separation. *RSC Advances,* 13, 16039–16046.
9. Yin, P., Hu, S., Qian, K., Wei, Z., Zhang, L. L., Lin, Y., Huang, W., Xiong, H., Li, W. X., & Liang, H. W. (2021). Quantification of critical particle distance for mitigating catalyst sintering. *Nature Communications,* 12, 251162.
10. Yang, S. J., Kim, T., Im, J. H., Kim, Y. S., Lee, K., Jung, H., & Park, C. R. (2012). MOF-derived hierarchically porous carbon with exceptional porosity and hydrogen storage capacity. *Chemistry of Materials,* 24, 464–470.
11. Huang, Y., Chen, Y., Xu, M., Ly, A., Gili, A., Murphy, E., Asset, T., Liu, Y., De Andrade, V., Segre, C. U., Deriy, A. L., De Carlo, F., Kunz, M., Gurlo, A., Pan, X., Atanassov, P., & Zenyuk, I. V. (2023). Catalysts by pyrolysis: Transforming metal-organic frameworks (MOFs) precursors into metal-nitrogen-carbon (M-N-C) materials. *Materials Today,* 69, 66-78.